II - VELOCITY FIELD AND MAGNETIC FIELD

https://doi.org/10.1017/S0074180900198766 Published online by Cambridge University Press

MAGNETIC FIELDS IN DENSE REGIONS

CARL HEILES
1989-1990 Visiting Fellow, Joint Institute for Laboratory Astrophysics
University of Colorado, Boulder CO 80309-0440 USA

ALYSSA A. GOODMAN
University of California, Berkeley, CA 94720 USA

CHRISTOPHER F. MCKEE
University of California, Berkeley, CA 94720 USA

ELLEN G. ZWEIBEL
University of Colorado, Boulder CO 80309-0440 USA

This paper concentrates on reviewing magnetic fields in dense regions; see Heiles (1988, 90) for a review of fields in diffuse regions. The past few years have increased our observational knowledge of magnetic fields in dense regions by an enormous factor—not because there are many measurements, but because we started from zero. The observable is polarization, which is small and subject to systematic errors. The fact that the advances have occurred only recently is a result of several factors: technological development; the interest and commitment of experimentally-minded astronomers; and the maturing of molecular and infrared astronomy to the point that really new results require either new insights or more difficult techniques.

This paper is a severe condensation of a more complete observational review (Heiles *et al.* 1990), which has an accompanying theoretical review denoted herein as Paper II (McKee *et al.* 1990). Previous observational reviews (Crutcher 1988, Troland 1990) summarize all existing observational results; here we cover results for only a few objects, but discuss them extensively. A word on notation. Equation (II 4.2) means equation (4.2) in Paper II. We use $\vec{B}$ to designate both the direction and magnitude of the magnetic field, $\widehat{B}$ to designate the direction alone (within the two-fold ambiguity of 'which way the vector points'), and B to designate the magnitude alone. The subscripts $\|$ and $\perp$ designate the line-of-sight and the plane-of-the-sky components, respectively.

E. Falgarone et al. (eds.), Fragmentation of Molecular Clouds and Star Formation, 43–60.

1. MANIFESTATIONS OF MAGNETIC FIELDS IN DENSE CLOUDS

1.1. Zeeman splitting.

The Zeeman effect arises from the coupling of an atom's or a molecule's magnetic moment with an external magnetic field. For any species with an unpaired electron spin the splitting $\Delta\nu_Z \sim 2$ Hz μG^{-1}, while for the much more common case of no unpaired electron spin but non-zero nuclear magnetic moment, such as H_2O, the splitting is smaller by roughly the ratio of the proton mass to the electron mass.

Under essentially all interstellar conditions except in OH masers, $\Delta\nu_Z \ll \Delta\nu$, where $\Delta\nu$ is the line width. This makes Zeeman splitting very difficult to detect. Success is favored by a species with both a large magnetic moment and a low line frequency (which increases the ratio $\Delta\nu_Z/\Delta\nu$), and also (of course!) by a high field strength. In this usual case, only the line-of-sight component $B_{||}$ is obtained and all measured splittings must be adjusted for the projection factor to derive the full field strength. The median correction factor is $B = 2B_{||}$ (Heiles and Troland 1982).

To date, the Zeeman effect has been detected from only four species in the interstellar medium: H I, OH, C_2S (Güsten and Fiebig 1990), and H_2O (Fiebig and Güsten 1989). B ranges from a few μG in H I to over 40 mG in H_2O masers.

The unpaired electron and low transition frequencies make OH the best tracer of magnetic fields in molecular regions. But just how well does OH trace H_2? The answer is not clear. In clouds that are not too dense, both observations and theory imply that OH is a good tracer of H_2. However, in cold dense clouds there are no observational indications, and theory implies that OH is *not* a good tracer of H_2.

Observationally, for moderate extinctions of < 7 mag the fractional abundance of OH with respect to H (total H, H I + $2H_2$) $X_{OH} \approx 4 \times 10^{-8}$ (Crutcher 1979). The major observational work that extends the range of *column* density as high as 7 mag is the detailed study of the ρ Oph dark cloud by Myers *et al.* (1978); this study finds the corresponding *volume* density to be $n_H \approx 2500$ cm^{-3}. Crutcher (1988) argues that OH traces n_H up to $\sim 3\times10^4$ cm^{-3} in TMC-1, but in our opinion this argument needs to be better substantiated and to be made quantitative. Theoretically, in clouds that are not too dense starlight dominates the ionization and is involved both in the production and destruction of many molecules. Under these conditions X_{OH} is predicted to be roughly independent of n_H for the range $250 < n_H < 1000$ cm^{-3}, although X_{OH} does depend on temperature, particularly for $T \gtrsim 50$ K (van Dishoeck and Black 1986). The way in which X_{OH} varies with n_H should be reliably predicted by the theory, but the actual theoretical value of X_{OH} depends on the exact process responsible for its formation (see below), which is uncertain; thus the theory cannot be expected to accurately reproduce the absolute abundance of OH. It seems reasonable to use the observations as a guide and extend the upper limit of the range of n_H from 1000 to at least 2500 cm^{-3}.

At high densities we must rely on theoretical astrochemical calculations. The question of what constitutes a 'high' density depends on the degree to which

starlight is excluded, which in turn depends on the degree of nonuniformity of a cloud, and in particular its porosity. The absence of starlight makes a big difference because the sequence of reactions that form OH involves ion-molecule reactions, whose rate is limited by the ionization rate. Without starlight, ionization results from cosmic rays, which to first order makes n_{OH} independent of n_{H_2} (Herbst and Klemperer 1973). Calculations that include a more complete set of reactions (e.g. Leung *et al.* 1984) indicate a weak dependence, roughly $n_{OH} \propto n_{H_2}^{0.2}$. Recent uncertainties in the exact process by which OH is actually produced (Lepp, Dalgarno, and Sternberg 1987; Gredel *et al.* 1989) affect the absolute abundance of OH but should not affect this approximate result that n_{OH} is almost independent of n_{H_2}.

The independence of n_{OH} with respect to n_{H_2} is definitely not universally true at very high densities. Theoretically, high-temperature regions should produce copious amounts of OH. High temperatures can be produced by shocks, either with magnetic fields (Draine and Katz 1986) or without (Mitchell and Watt 1985); X_{OH} can be much higher than usual with shock velocities of somewhat less than 10 km s^{-1}. In OH masers, X_{OH} is high and $n_H \sim 10^7$ cm^{-3}; the high OH abundance can be understood only if these regions have been subjected to high temperatures.

1.2. Polarization of radio spectral lines arising from radiative transfer effects.

1.2.1. Emission lines: linear polarization. Linear polarization provides information on $\widehat{B}_\perp$, the projection of $\widehat{B}$ on the plane of the sky. The physical mechanism that produces linear polarization rests on the fact that π and σ components, which are orthogonally polarized, have different directional dependencies on their interaction with radiation when an external magnetic field orients the quantization axis. To obtain a significant population difference the molecule must be subject to a sufficiently intense anisotropic radiation field and the collisional rate must not be too high. In addition, the Zeeman splitting must be larger than the collisional and the spontaneous emission rates, but small compared to the line width. These conditions are easily satisfied for many transitions.

To discuss the predicted observables we consider two illustrative examples introduced by Kylafis (1983a) in which the anisotropy is provided by the velocity field. The velocity field is symmetric with respect to the z axis. In the 1-d example, the cloud expands in the z direction with uniform velocity gradient. In the 2-d example, the cloud expands axisymmetrically with no motion in the z direction. The magnetic field is parallel to the axis of symmetry and is perpendicular to the line of sight.

a. Intensity: Kylafis (1983a) provided solutions over the full range of physical parameters for his two examples, but restricted the treatment to a two-level system. Deguchi and Watson (1984) extended the treatment to the full rotational ladder for CO and CS, and found that the polarization was smaller than for the two-level case by a factor ~ 2; we use their results here.

https://doi.org/10.1017/S0074180900198766 Published online by Cambridge University Press

The *fractional polarization*, denoted as $p_l = (U^2 + V^2)^{1/2}/I$, depends sensitively on C/A, the ratio of collisional rate to Einstein A, and also on the optical depth. As $C/A \to 0$, $p_l \tilde{\to} 0.10$; as C/A increases, p_l decreases significantly. The linearly *polarized intensity* $P_l = (U^2 + V^2)^{1/2}$ peaks at $C/A \sim 1$, at which point $p_l \sim 0.01$ for the 2-d and 0.03-0.12 (depending on the viewing angle) for the 1-d case.

These two simple examples show that p_l depends extremely sensitively on the velocity field. Simply going from 1-d to 2-d reduces the polarization to the point of being observable only with difficulty. It seems reasonable to conclude that for more realistic velocity fields the polarization will be very small indeed.

b. Direction: The polarization is either parallel or perpendicular to $\widehat{B}_\perp$, but it is not so easy to determine which. Again we consider the two examples of Kylafis (1983a). Consider the behavior as a function of α, the direction of the magnetic field. In the 1-d case, the polarization is perpendicular to the magnetic field for $54.7° < \alpha < 125.3°$, and parallel otherwise. In contrast, the 2-d case is *precisely opposite*.

In the absence of calculations for other, more realistic situations, we can only speculate. The direction of polarization is a sensitive function of the details of the velocity field. It seems likely that in more complicated cases the polarization direction might change direction rapidly with position, both on the sky and along the line of sight, and this should lead to much smaller p_l than is predicted for the simple situations. In this spirit, the negative results of attempts to observe polarization by Wannier, Scoville, and Barvainis (1983) and by Lis *et al.* (1988) come as no surprise.

1.2.2. Absorption lines: linear and circular polarization. a. Linear polarization: Absorption lines seen against a background source are polarized by the same mechanism as emission lines. But there is an additional possibility. If the source is nearby, so that it subtends an appreciable solid angle as seen by the gas, then the source itself provides a non-isotropic source of radiation. This radiation can be either at the frequency of the line or at other relevant frequencies for excitation of the line such as far-IR for the OH molecule (Burdyuzha and Varshalovich 1972). This anisotropic radiation can affect the level populations to a greater degree than other local physical conditions if the source is strong. An extreme example is circumstellar material, in particular SiO masers.

Two idealized examples by Kylafis (1983b) produced detectably large polarization, and it seems worth making a serious observational effort to detect the linear polarization of absorption lines. Interpretation of results will not be without ambiguity, because as in the case of polarized emission lines the polarization is either parallel or perpendicular to $\widehat{B}_\perp$, depending on geometry. The requirement that the background source subtend a large solid angle is crucial to the mechanism, and observers should select sources for which other evidence favors this geometry.

b. Circular polarization: Circular polarization can exist whenever linear polarization can be produced by the mechanisms discussed above, which rely on differing

opacities for the polarizations that are parallel and perpendicular to $\widehat{B}_\perp$ (the 'optical axes'). These opacities are the imaginary part of the index of refraction. According to the Kramers-Kronig dispersion relation, this inevitably leads to different phase velocities for orthogonal linear polarizations that are aligned along the optical axes. This turns linear polarization into circular polarization by a process that is similar to Faraday rotation, which occurs when the phase velocities are different for the orthogonal circular polarizations.

First, consider a linearly polarized background source. If the polarization direction is *not* parallel to either optical axis, then the wave can be decomposed into two waves in both axes. The differing phase velocities then produce elliptical polarization; the intensity of the circular component varies sinusoidally with distance along the direction of propagation. The polarization always changes sign across the line center, and looks similar to signature of the Zeeman effect. This is known as 'linear birefringence' (Kylafis and Shapiro 1983). V can be comparable to the change in linear polarization.

Next, consider an unpolarized background source. Here, the differing opacities produce linear polarization within the cloud. This polarization lies along one of the optical axes, so there is no possibility for circular polarization. However, if the direction of $\widehat{B}_\perp$ changes along the line of sight—the field 'twists' along the line of sight—then the optical axes follow the twist and linear birefringence can occur. The circular polarization depends on the amount of twist. For typical cases we expect $p_c \lesssim p_l^2$, because the circular polarization is a second-order effect.

c. Fake Zeeman splitting: In the latter 'unpolarized background source' case, p_c should be typically so small that it would be very difficult to detect, and we would thereby recommend that observers concentrate on other, less difficult observations. Nevertheless, the effect may loom large in importance because it mimics—and can easily be mistaken for—the Zeeman effect. The Zeeman effect produces small p_c, about $1.5\Delta\nu_Z/\Delta\nu$. This amounts to a percent or less in many cases, which is small enough to be produced by linear birefringence. If so, linear polarization should also be present.

1.2.3. Polarization in masers. a. Zeeman splitting: Fiebig and Güsten (1989) have detected weak circular polarization in H_2O masers for one maser in each of four H II regions and derive typical $B_\parallel \sim 35$ mG; H_2O masers sample densities of 10^8 to 10^{10} cm^{-3} (Elitzur, Hollenbach, and McKee 1989; EHM). The circular polarization $p_c \sim 0.001$, which is extremely small. If linear polarization is present at the level of a few percent, the circular polarization could be a result of linear birefringence (section 1.2.2*b, c*). Future observations should include all Stokes parameters, which makes the task more difficult.

For OH masers associated with H II regions, Reid and Silverstein (1990) have compiled and assessed many measurements. Field strengths range up to 7 mG and average 3.6 mG. OH masers sample densities of 10^6 to 10^8 cm^{-3} (Reid and Moran 1981). If we ignore the possibility that the H_2O and OH field strengths are biased towards high values because of observational selection effects, then we conclude, very roughly, that in this regime $B \propto n^{1/2}$.

Reid and Silverstein come to a remarkable conclusion: the ***directions*** of the fields in OH masers are systematically aligned over large segments of the Galaxy. This indicates that the field direction is largely preserved during the contraction of clouds to high volume densities. This is surprising, because during this contraction process one would expect the competing effects of gravitation, angular momentum, and shocks to randomize the field in the dense cloud with respect to the surroundings. We discuss a particular example, Orion, below in section 2, and conclude that the coincidence of the field directions in Orion and the Galaxy may be accidental; this makes the conclusion of Reid and Silverstein either suspect or even more remarkable.

b. Linear polarization: Linear polarization is produced by the same basic mechanism as discussed above in section 1.2.1. The production of linear polarization in J=1–0 transitions requires that several constraints on ratios of pumping rates, decay rates, and Zeeman splitting be satisfied (Goldreich, Keeley, and Kwan 1973). However, extremely recent calculations by Deguchi and Watson (1990) and Nedoluha and Watson (1990) show that for higher-J transitions, such as in H_2O masers, the constraints are more severe. The existence of detectable linear polarization in H_2O masers implies field strengths of $\sim$ 30 mG, which is commensurate with the few results obtained directly from Zeeman splitting of H_2O masers.

1.3. Linear polarization caused by aligned grains.

Optical starlight is almost universally linearly polarized, to a degree that increases with extinction. The polarization arises from absorption by systematically oriented dust grains. Only magnetic orientation is sufficiently general and powerful to provide the universality, although in individual circumstances other agents, such as gas streaming or photons, may dominate (e.g. section 2.2). An excellent contemporary review of these matters is given by Hildebrand (1988).

In magnetic alignment, a needle-like grain spins primarily end-over-end around an axis that is parallel to $\widehat{B}$. The polarization that is most strongly absorbed by this field of systematically aligned grains lies along the longest projected grain area, which is perpendicular to $\widehat{B}_\perp$. Therefore, the observed linear polarization of absorbed light is parallel to $\widehat{B}_\perp$. The alignment also produces linear polarization of the grains' thermal emission at far-infrared and sub-mm wavelengths, which is perpendicular to $\widehat{B}_\perp$.

2. OBSERVATIONAL EXAMPLES: ORION

The Orion region occupies a place of central importance because it is the nearest region of massive star formation. Orion A is a 'blister' H II region, protruding from the near side of a dense molecular cloud within which the current star formation activity is occurring.

2.1. $B_{\|}$ from Zeeman splitting. Volume densities sampled by the different observations range from $\gtrsim 400$ to $\sim 10^9$ cm^{-3}, a range of about 6 orders of magnitude, and the total magnetic field strengths B range from ~ 0.05 to ~ 40 mG, a range of about 3 orders of magnitude. Thus, very roughly, $B \propto n^{1/2}$.

a. Ambient gas: The ambient gas on the near side of the H II region is sampled by absorption lines. The H I absorption line comprises two velocity components. In our opinion, this H I is not in the photodissociation region (PDR) and does not directly abut the H II region. We support our opinion by two facts. One, the H I velocities of ~ 0 and 6 km s^{-1} are 3 and 9 km s^{-1} more *positive* than the H II velocity, while the absorption gas is in front of the H II region and should be moving at *negative* velocity with respect to the H II region. Two, the H I is cold, but given the exciting stars for Orion the H I in the PDR should be warm (Tielens and Hollenbach 1985).

In the H I absorption lines, Troland, Heiles, and Goss (1989) mapped the field strength with 25″ resolution over most of the H II region, which occupies an area about 5′ in diameter. They found $B_{\|}$ to range from –43 to –107 μG. In both OH and H I absorption lines, Troland, Crutcher, and Kazès (1986) measured Zeeman splitting for a single spot on the eastern edge of the H II region; they obtained –125 and –49 μG, respectively. We adopt $B = -100$ μG, and if this uniformly fills a 5′-diameter circle, the magnetic flux is –2.0 mG arcmin^2.

b. The dense molecular gas: This gas lies on the far side of the H II region. The molecular 'doughnut' (Plambeck *et al.* 1982) is a disk of dense (up to $\sim 10^7$ cm^3) gas with outer diameter $\sim 44''$ and a hole in the middle. It surrounds IRc2 and expands at ~ 20 km s^{-1}. Its total mass is ~ 15 M$_\odot$, which seems to be too massive to have been ejected directly from IRc2. The expansion time scale (radius/velocity) ~ 3000 yr and the kinetic energy $\sim 5 \times 10^{46}$ erg, which amounts to $\sim 0.5\%$ of the luminosity of IRc2 in 3000 yr. Thus it is reasonable to consider the doughnut as being composed of ambient material that has been swept up—i.e., shocked—by less massive, faster-moving or high-temperature ejecta from IRc2.

There are two classes of H_2O maser, the 18 km s^{-1} ('low-velocity') flow and the 30-100 km s^{-1} ('high-velocity') flow (Genzel *et al.* 1981). The low-velocity masers lie in the plane of the doughnut and trace its outside with diameter $\sim 44''$; they have $n_H \sim 10^9$ cm^{-3} and $B \sim 30$ mG, corresponding to an Alfvén velocity $V_A \simeq 1.8$ km s^{-1}. The high-velocity masers lie on the axis of the doughnut and are probably the equivalent of Herbig-Haro objects.

Most of the OH masers lie within 8″ of IRc2 and have velocities within 18 km s^{-1} of IRc2 (Johnston, Migenes, and Norris 1989). Thus it seems that the OH masers trace the *inside* of the doughnut, because both the velocities and gas densities match. The OH masers have $n_H \sim 10^7$ cm^{-3} and $B \sim 1.4$ mG, which gives $V_A \simeq 0.8$ km s^{-1}. Comparing the H_2O and OH masers implies that the Alfvén velocity is constant to within a factor ~ 2, or *very* roughly, $B \propto n_H^{1/2}$.

How are the masers excited? EHM have suggested that H_2O masers arise in shocks. Their calculations were for the case of fast, dissociative shocks, but the conditions in slower, non-dissociative shocks can be similar, so it is likely that the

low-velocity H_2O masers arise in shocks. Much of the emission in non-dissociative shocks occurs near the velocity of the *unshocked* gas, where the heating due to ambipolar diffusion is greatest. However, in order to get saturated maser emission in masers of the observed size (which is comparable to the shock thickness), the density must be of order 10^9 cm^{-3} (EHM); this suggests that the maser emission occurs at the density, and hence the velocity, of the *shocked* gas. The location of the H_2O masers at the outer perimeter of the doughnut is consistent with the idea that they are in recently shocked gas.

The OH maser is a ground state transition, so exciting it does not require the temperature to be above several hundred degrees as does the water maser. (Production of OH requires either high temperatures [section 1.1] or photodissociation of H_2O, though.) The location of the OH masers at the inner edge of the doughnut is consistent with either radiative pumping or with weak shocks due to variations in the wind luminosity of IRc2. However, we are left with the puzzle as to why the pressure in the H_2O masers is so much greater than that in the OH masers, even though their radial velocities are the same.

c. Connection of the ambient to the dense gas: The OH masers see the magnetic field near the inside of the doughnut, ~ -1.4 mG, and the H_2O masers at the outside, ~ -30 mG. We don't know how the field strength varies within the doughnut, but if the average field strength is –5.4 mG then the doughnut, which we take as a circle 44″ in diameter with a 16″ diameter hole, contains the same magnetic flux as the ambient gas, ~ -2.0 mG arcmin^2.

There is, in fact, no reason to assume that the fluxes are equal because the ambient-medium flux was obtained from the H I absorption observations and thereby depends on the size of the H II region, which is determined by completely different considerations. However, if the fluxes are, in fact, equal then the field lines can connect the dense gas to the ambient gas, while satisfying the constraint $\nabla \cdot \vec{B} = 0$, without bending unduly sharply. This is because the H II region is roughly spherical (Balick, Gammon, and Hjellming 1974), so that as the field lines diverge from the doughnut, which is located behind the H II region, to the ambient gas, which is located in front, they need not bend by more than 30°.

The *sign* of $B_\parallel$ is negative for *all size scales.* This would seem to be a single example of the general trend for OH masers that the maser field directions reflect the Galactic or ambient field directions (section 1.2.3*a*.). However, the situation is not quite so clear-cut: Zeeman observations of OH in absorption against Orion B (NGC2024), only 4 degrees away from Orion A, show a *positive* field (Heiles and Stevens 1986). Thus, Orion A and Orion B cannot both reflect the ambient Galactic field. We suspect that the last word has not yet been written concerning the general trend for OH maser fields to reflect the ambient Galactic field.

2.2. $\widehat{B}_\perp$ from linear polarization. Next, we consider linear polarization, which indicates the direction of $\widehat{B}_\perp$. Polarization of the far-IR continuum emission from dust grains has been measured with 40″ angular resolution by Novak *et al.* (1989) and Gonatas *et al.* (1990), and that of mm-wave emission with about 22″ resolution

by Barvainis, Clemens, and Leach (1988) and Novak, Predmore, and Goldsmith (1990). Position angles for the far-IR and mm wavelengths are similar, which means that the polarization is produced by aligned grains. If the grains are oriented by the magnetic field, then the position angle of the field as derived from dust, $\theta_{B,dust}$, is about 110°.

Aitken *et al.* (1985) made spectropolarimetric observations of the diffuse mid-IR (8-13 μm) continuum with 4″ angular resolution on six IR sources within $\sim$ 12″ of IRc2. For all positions except IRc2, the spectral dependence of the polarization follows that of the overall grain opacity, which means that the polarization is produced by absorption of aligned grains; polarization directions differ from those at shorter wavelengths, where polarization results from scattering (Werner, Dinerstein, and Capps 1983). Importantly, the position angle varies considerably among the six positions: the polarization vectors all tend to point towards IRc2. Aitken *et al.* use this fact to argue that the grains are oriented *not* by the magnetic field, but by the photons from IRc2.

Whatever the mechanism of grain alignment, the observational fact is that 4″ resolution reveals structure in the mid-IR polarization. Thus the alignment direction of the grains changes on scales of a few arcsec, and the coarser angular resolution that has been used at far-IR and mm wavelengths is inadequate. For the BN position, the values of $\theta_{B,dust}$ derived from the mid-IR and far-IR agree, possibly because the average of the mid-IR Stokes parameters over the 40″ far-IR beam yields a position angle of 109° (Novak *et al.* 1989).

$\theta_{B,dust} \approx 110°$ is in very good agreement with the position angle of $\sim$ 100° for *optical* polarization of background stars over an area $\sim$ 1° in extent. Optical polarization indicates the field direction in the ambient matter surrounding the dense molecular cloud. Thus we obtain a nice picture, one that is consistent with the Zeeman results: the field direction in the dense cloud is similar to that in the immediately-adjacent medium.

Position angles describe several other phenomena in the innards of Orion, and we might expect them to be related to the local direction of the field. These phenomena include H_2O maser polarization and the orientations of various dynamical or structural features. We exhibit them in Figure 1 and discuss them in the following paragraphs:

(1) The low-velocity H_2O masers tend to lie on a line having position angle $\theta_{line} \sim 30°$ (Knowles and Batchelor 1978). EHM predict that the maser luminosity $\propto B_{0\perp}^4$, where $B_{0\perp}$ is the component of the preshock magnetic field perpendicular to the shock velocity. The shock moves radially outward from IRc2. $B_{0\perp}$ is largest, and the masers should be strongest, where the shock moves orthogonally to $\widehat{B}_\perp$. Thus θ_{line} should lie 90° away from $\theta_{B,dust}$; the actual value is only $\sim$ 10° different.

(2) The group of most intense OH masers, populations 1 and 2 of Norris (1984), lie on a line having position angle $\sim$ 60°. This differs by 40° from the value expected from the EHM theory, which may not apply to OH masers. The OH masers lie toward the inside of the doughnut, while the H_2O masers lie on the outside; the field directions may differ in these regions.

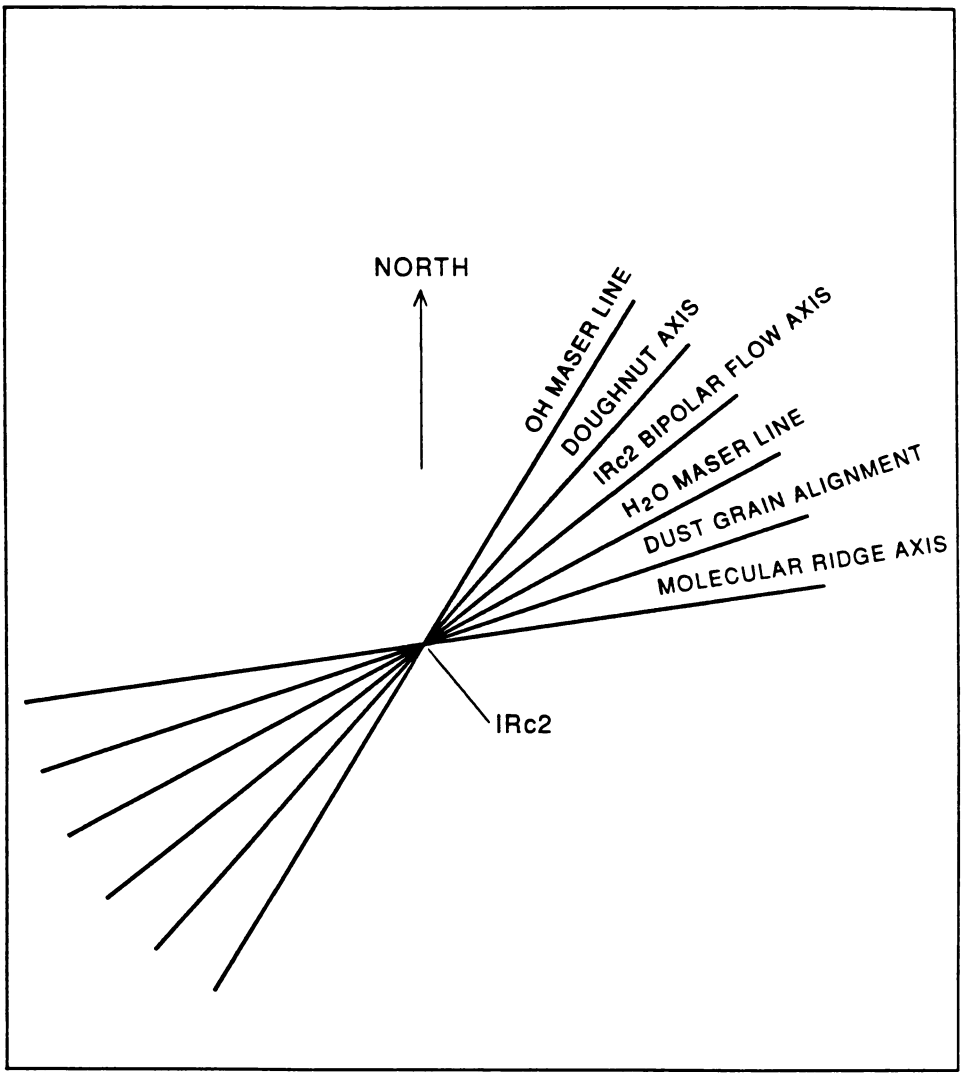

Figure 1. Directions of $\widehat{B}_\perp$ near IRc2 in Orion derived from the possible indicators discussed in the text. Aside from observational uncertainties, differences might be caused by changes in $\widehat{B}_\perp$ with position.

(3) On the very smallest scale, the position angle of the bipolar flow from IRc2 is $\sim 130°$; this is our estimate using the SO map of Erickson *et al.* (1982) and the SiO map of Wright *et al.* (1983). This is only about 20° from $\theta_{B,dust}$.

(4) Judging from the map of Vogel *et al.* (1984), the axis of the molecular doughnut has position angle 140°, $\sim 30°$ from $\theta_{B,dust}$.

https://doi.org/10.1017/S0074180900198766 Published online by Cambridge University Press

(5) On the much larger scale of $\sim 0.5°$ (~ 4 pc), the 'molecular ridge' in which the Orion complex is imbedded has a position angle of $\sim 10°$, and it contains filaments running along its length (Bally *et al.* 1987). This is nicely aligned (perpendicularly) to $\theta_{B,dust}$.

Figure 1 shows that the inferred $\theta_B = 130° \pm 20°$. It is quite well defined given the uncertainties in measurement and interpretation. This is particularly true because the projection from 3-d to the 2-d plane-of-the-sky tends to amplify angular differences.

We conclude that position angles of various structural features may provide significant information on the magnetic field. However, we need much more than a statistical sample of one H II region! There is much to be done in the way of further observations, both on Orion itself and on other H II regions. We again remark that the mid-IR results show that high angular resolution is required, and that alignment of dust grains may occur by nonmagnetic processes.

3. OBSERVATIONAL EXAMPLES: DERIVING $\vec{B}$

Myers and Goodman (1990; MG90) have devised a method to almost completely specify the uniform component of $\vec{B}$. Consider the total magnetic field $\vec{B}$ at any point in space to be the vector sum of a straight 'uniform' field, $\overrightarrow{B_0}$, and a spatially varying, nonuniform field, $\overrightarrow{B_r}$. Individual Zeeman observations sample $B_\parallel$ and provide estimates of both $B_{\parallel,0}$ and the dispersion of the line-of-sight component of B_r, $\sigma_{B_\parallel}$. Similarly, optical polarization maps provide the mean position angle of $\widehat{B}_\perp$, $\langle\theta_B\rangle$, and its dispersion σ_{θ_B}.

$B_{\perp,0}$ cannot be derived directly from the measured polarization because too little is known about the grain alignment process. Nevertheless, its mean value can be determined statistically by using a model. The model predicts an observed distribution of θ_B in which the ratio $B_{\perp,0}/\sigma_{B_\perp}$ is the only free parameter. In most cases, the expected distribution is well-represented by a Gaussian, and σ_{θ_B}, the 1-σ width of the distribution, is a function only of the ratio $B_{\perp,0}/\sigma_{B_\perp}$ and N, the number of independent samples of B_r along the line of sight. The model also relates $\sigma_{B_\parallel}$ to $\sigma_{B_\perp}$. The resulting $B_{\perp,0}$, together with $B_{\parallel,0}$ and $\langle\theta_B\rangle$, provide $\overrightarrow{B}_0$ within a two-fold directional ambiguity. $\sigma_{B_\parallel}$ and $\sigma_{B_\perp}$ provide B_r, and combining B_0 and B_r in quadrature yields B.

Models include one for which $\overrightarrow{B_r}$ is essentially two-dimensional, resulting from Alfvén waves (Zweibel 1990; MG90), and a 'turbulent' field model, in which $\overrightarrow{B_r}$ is distributed isotropically in three dimensions (MG90). The isotropic model may be unrealistic because transverse fluctuations undergo weaker nonlinear damping than do aligned or longitudinal fluctuations. An ideal model would incorporate both density and magnetic field fluctuations using the concepts first enunciated by Chandrasekhar and Fermi (1953). In any model there is the practical problem of separating fluctuations from systematic gradients.

We mention two important caveats. First, the Zeeman and polarization observations highlight different portions of the cloud unless care is exercised in selecting the statistical samples. Zeeman observations emphasize the regions of high $B_{\|}$, which tend to be those of high n; polarization observations are most easily obtained in regions of low extinction, which tend to have low n. Second, the result depends on the model used to describe the fluctuations in $\vec{B}$. Magnetic fluctuations are not inherently isotropic, so the relation between $\sigma_{B_{\|}}$ and $\sigma_{B_{\perp}}$ depends on $B_{\|,0}/B_0$, which is itself derived from the model. Finally, in the best of worlds the model is consistent both with basic physical principles and with their application to the specific physical conditions in the region.

In the dark cloud Lynds 204 (L204), Heiles (1988) has made H I Zeeman measurements on a grid of 27 positions covering approximately a 6 by 15 pc area. McCutcheon *et al.* (1986) have made well-sampled optical polarization measurements. These data are sufficient to apply the technique. We quote results for the $N = 1$ case and the self-absorption component only, which should be representative of the denser parts of the cloud.

MG90 find $B_{\|,0} = 7.6$ μG and $\sigma_{B_{\|}} = 4.7$ μG. They use the isotropic model and find $B_{\perp,0} = 16.9$ μG, $B_0 = 18.5$ μG, $B_r = 8.1$ μG, and $B = 20.2$ μG. L204 is in approximate virial equilibrium, and this field value is in reasonable agreement with the expectations from Paper II (Heiles 1988). Heiles finds two correlations, one between the cloud shape and line-of-sight velocity and one between $B_{\|}$ and line-of-sight velocity, which allow a resolution of the two-fold ambiguity in $\widehat{B}_{0,\perp}$ and $\widehat{B}_0$. The correlations also imply the presence of large-amplitude Alfvén waves, which may make the isotropic model inapplicable.

4. OBSERVATIONAL EXAMPLES: THE VIRIAL THEOREM AND CLOUDS

4.1. The virial theorem: observational considerations

Many observational treatments of molecular clouds rely on the virial theorem, written for a spherical cloud of uniform density and mass M:

$$|W| + 3P_0V = 2T + \mathcal{M} \ , \tag{4.1}$$

where W is the gravitational potential energy $-3GM^2/5R$, $3P_0V$ is the external pressure term including turbulent pressure, T the total kinetic energy $0.27M\,\Delta v^2$ ($2T$ is $3\bar{P}V_{cl}$), and $\mathcal{M}$ the total *net* magnetic energy (including surface terms) $0.1B^2R^3$, where the factor 0.1 comes from Tomisaka, Ikeuchi, and Nakamura (1988). Here we use the observationally-oriented Δv, which is the line width at half peak intensity; it is related to the theoretically-oriented one-dimensional velocity dispersion, σ, by $\sigma^2 = 0.18\ \Delta v^2$.

https://doi.org/10.1017/S0074180900198766 Published online by Cambridge University Press

This allows the overall equilibrium to be described in terms of global cloud parameters, which can be derived directly from observational data. This is a 'minimalist' approach, because it avoids dealing with the internal structure of clouds. The problem is the uncertainties in the virial terms. This problem is well exemplified by our discussion of the B1 cloud below in section 4.3 and, apart from matters such as surface terms and nonuniform cloud structure, involves three specific observational quantities: the assumed distance, the conversion of $B_{\|}$ to B, and the determination of the true H_2 content.

The distance uncertainty can be very serious and should never be ignored or minimized.

The second problem is a matter of projection angle. We usually measure $B_{\|}$ instead of B. For a large sample $\langle B \rangle = 2B_{\|}$. However, in any individual case we can only be sure that $B \geq B_{\|}$. The matter is important, because the magnetic term in the virial theorem $\mathcal{M} \propto B^2$, and the arbitrary use of the relation $B = 2B_{\|}$ increases $\mathcal{M}$ by a factor of 4 over its minimum value.

The third problem involves determination of the volume density n_{H_2} or, equivalently, the column density N_{H_2} or cloud mass M. Derived values of neither volume nor column density are generally accurate within a factor of two or three. Turner and Ziurys (1988) provide a contemporary summary of this problem.

Factors of two are good from the standpoint of astronomical accuracy but inadequate for a definitive discussion involving the virial theorem, as we shall see in our discussion of B1 (section 4.2) below. If $\mathcal{M}$ is important, then all terms in the virial theorem are likely to be comparable, and the uncertainties allow virial equilibrium whether $\mathcal{M}$ is included or not.

4.2. B1: Observations.

B1 is, to our knowledge, the dark cloud about which most is known from the combined standpoints of structure and magnetic field, and represents the best example for application of the virial theorem. B1 is a well-defined cloud in the Perseus region which has been mapped in several molecular transitions, including ^{13}CO with 4.4 arcmin resolution by Bachiller and Cernicharo (1984); OH with 3 arcmin resolution by Goodman *et al.* (1989; hereafter GCHMT); and NH_3 with 40 arcsec angular resolution by Bachiller, Menten, and del Río-Alverez (1990, hereafter BMdR). For these molecules—^{13}CO, OH, and NH_3—the sizes decrease and the line widths decrease monotonically. This is a reasonable result, because the three molecules trace increasingly dense regimes of H_2 volume density, and according to 'Larson's laws' (Larson 1981; Solomon *et al.* 1987), size $\propto n_{H_2}^{-1}$ and line width $\propto n_{H_2}^{-1/2}$.

The appearance of B1 in these three molecules is depicted in Figure 2. As the angular scale gets smaller B1 gets more complicated. We define the cloud *core* as the $\sim$ 3′-diameter portion of the cloud highlighted by the NH_3 lines. The core contains an IRAS source that exhibits an apparent outflow, and thus is a protostar or newly-formed star. The cloud core consists of two or three condensations, which

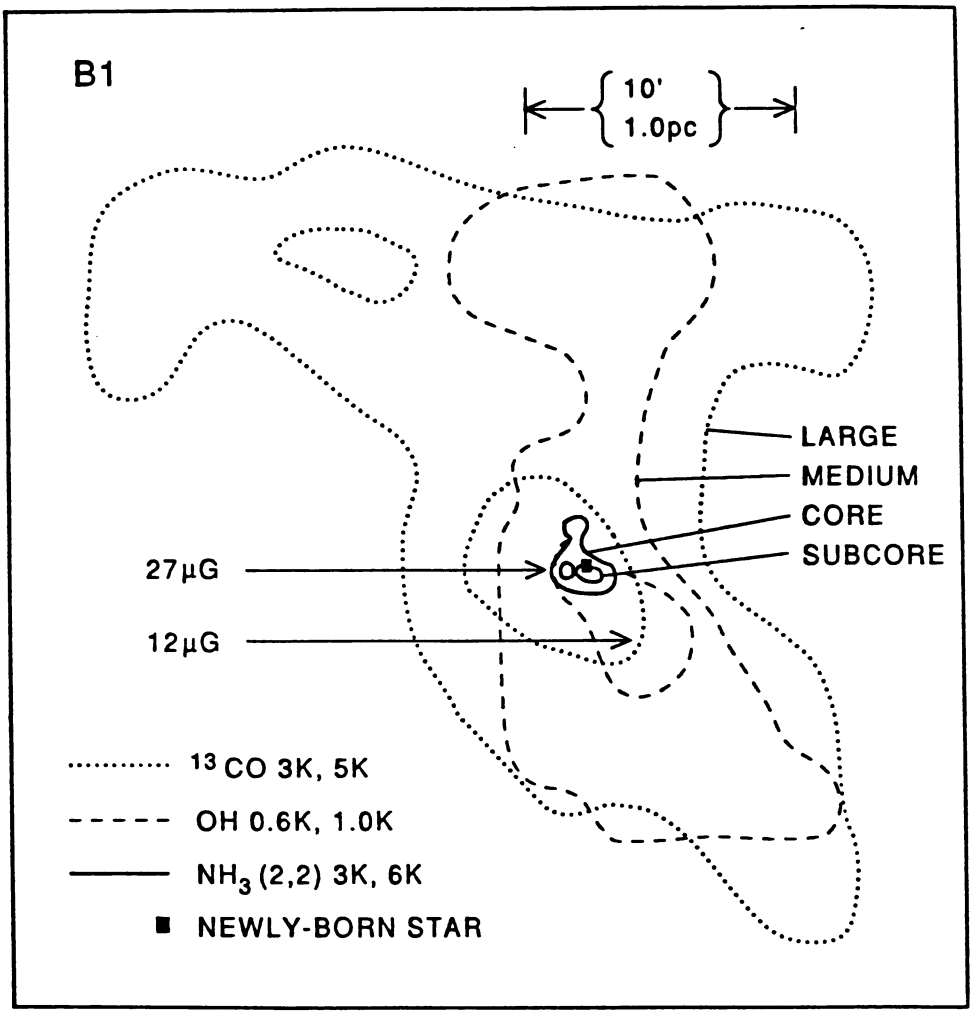

Figure 2. B1 as observed in ^{13}CO, OH, and NH_3. The three molecules highlight increasingly smaller size scales (see text). Only two contours are shown for each molecule, one near the peak and one about half the peak intensity. The four size ranges, ranging from 'large' to 'subcore', are indicated, as are the two $B_{\|}$'s derived from OH Zeeman splitting. There are several young stars in the region; we show only the one located in the core.

we define as *subcores*, separated by about 1.2 arcminutes, in which $n_{H_2} \sim 4 \times 10^4$ and 8×10^4 cm^{-3}. If these subcores themselves have smaller substructure, it would not have been resolved by existing observations.

https://doi.org/10.1017/S0074180900198766 Published online by Cambridge University Press

Zeeman splitting of the OH 1665 and 1667 MHz lines was measured by GCHMT and Goodman (1989). On the core, $B_{\|} \approx -27$ μG, while 4′ to the southwest $B_{\|} \approx -12$ μG (Figure 2). Goodman's (1989) off-core result of only −12 μG is less than half the field strength measured on the core, which implies that the field strength increases in the core. Further, if we were able to sample exclusively the dense core gas, then the measured field strength might be even greater than the −27 μG obtained from the OH, because as discussed in section 1.1 the OH may not sample the densest portions of the core.

The question of just how well OH traces high-density regions is a major one and deserves intense observational and theoretical attention.

4.3. The virial theorem applied to B1. Figure 2 depicts four size ranges of B1: 'large', 'medium', 'core', and 'subcore'. We have reasonably complete information on physical conditions for each size range, which allows us to evaluate the virial terms in equation (4.1) and other quantities. Unfortunately, we do not have a complete sample of $B_{\|}$ in the four size ranges, and there is always the annoying matter of converting $B_{\|}$ to B. We assume $B = 2B_{\|}$. For the medium size and core the observations provide $B_{\|} = -12$ and -27 μG, respectively. For the subcore we assume that $B_{\|}$ is the same −27 μG that it is for the core. This may well be incorrect, because $B_{\|}$ increases as we go from the medium size to the core, but it serves as a reasonably interesting example.

The external pressure term is not usually included in observational discussions, but it is important for the three smallest size ranges. Let P_0 be the external pressure at the boundary of each size range. At the boundary of the largest size range, P_0 should equal the ambient interstellar pressure, for which we adopt $P_0 = 1.6 \times 10^4 k_B$ (Paper II). For the smaller size ranges, we set P_0 equal to the total pressure of the gas in the next larger size, calculated from the line width and density. That is, we take $P_0 = \rho\sigma^2 = 0.18 \times 10^{10} \rho \Delta v_5^2$, which amounts to assuming that the velocity field is 'microturbulent'. This assumption is theoretically justified, because in the subcore the damping length of MHD turbulence is about 0.005 pc (equation II 4.2), which is 20 times smaller than the size of the subcore.

Table 1 gives numerical values for the virial terms. We emphasize that the accuracies are low. Virial equilibrium is easily achieved for any size by changing the mass by a factor of less than two, which is within the observational uncertainties. For all size ranges, the virial theorem is satisfied as well by excluding $\mathcal{M}$ as by including it, which is the inevitable consequence of the uncertainties and having all terms in the virial theorem comparable.

We now we forge ahead and discuss the stability of the virial equilibrium, temporarily assuming absolute accuracy. We do this with ratios of the mass to three different critical masses. Table 1 lists the cloud mass M in terms of the magnetic critical mass M_Φ (equation II 2.16), the Jeans (gravitational) critical mass M_J (equation II 2.12), and the combined magnetic/gravitational critical mass M_{cr} (equation II 2.19). All sizes have $M/M_\Phi > 1$ and are magnetically supercritical, which means that without gravity they would expand. Nevertheless, the magnetic field is crucial for the stability of the medium size and core. These have

TABLE 1

B1 AT VARIOUS SIZE SCALES

SIZE	$n(H_2)$ cm^{-3}	B μG	MASS $M_\odot$	$-W$ erg	$3P_0V$ erg	$2T$ erg	$\mathcal{M}$ erg	M/M_Φ	M/M_J	M/M_{cr}
Large[a]	900	-10^b	630	1.5(46)	.20(46)	3.0(46)	.07(46)	4.5	0.43	0.34
Medium[a]	2600	-24^c	120	1.5(45)	2.0(45)	2.3(45)	.30(45)	2.2	2.2	1.13
Core[a]	20000	-54^c	10	4.3(43)	2.4(43)	5.3(43)	1.6(43)	1.64	2.3	0.99
Subcore[d]	70000	-54^b	2.5	6.4(42)	3.8(42)	13.0(42)	1.1(42)	2.4	0.85	0.65

a. From GCHMT, taking R in their Table 2 as the cloud diameter.

b. Assumed. For the core, where B probably increases, this value is probably a lower limit.

c. Twice the measured value, to account for orientation to line of sight.

d. From Bachiller, Menten and del Rio-Alvarez (1990); these parameters apply to a single NH_3 subcore, and differ from the parameters given by those authors, which apply to the whole NH_3 core.

$M/M_J \approx 2.2$, which means that in the absence of the magnetic field they would be unstable to collapse. But M_{cr} includes the magnetic support, and these two sizes have $M/M_{cr} \approx 1$, which either removes the instability or makes it much less pronounced.

We emphasize again that the statements in the above paragraph are based on uncertain parameters. If we had used a more conventional definition of cloud radius, or different values for n_{H_2}, we would have reached different conclusions. Nevertheless, we are encouraged by the result $M/M_{cr} \approx 1$ for the core. The core has split into three subcores, and it also contains a protostar or new star. These are *observational* indications that the core of B1 is on the verge of instability. With $M/M_{cr} \approx 1$, we have a *theoretical* indication that it is close to instability. This argues that our numerical estimates in Table 1 are reasonably accurate.

ACKNOWLEDGMENTS

We thank Rafael Bachiller, Vladimir Burdyuzha, Dick Crutcher, Rolf Güsten, Roger Hildebrand, Terry Jones, Karl Menten, Mark Reid, and Tom Troland for providing unpublished material; and John Bally, Gary Fuller, Miller Goss, Roger

Hildebrand, Terry Jones, Nick Kylafis, Phil Myers, Barry Turner, and Paul van der Werf for instructive discussions. CH was supported in part by NSF grant 443836-21705. AG is supported in part by a President's Fellowship at the University of California, Berkeley. CFM's research is supported by NSF grant AST-8918573; his research on star formation is supported in part by a NASA grant to the Center for Star Formation Studies. EAZ was supported in part by NSF grant ATM85-60032 and the Institute for Theoretical Physics NSF grant PHY89-04035.

REFERENCES

Aitken, D.K., Bailey, J.A., Roche, P.F., and Hough, J.M. 1985, *M.N.R.A.S.*, **215**, 815.
Bachiller, R., Menten, K.M., and del Río-Alverez, S. 1990, *Astron. Ap.*, **000**, 000.
Bachiller, R. and Cernicharo, J. 1984, *Astron. Ap.*, **140**, 414.
Balick, B., Gammon, R.H., and Hjellming, R.M. 1974, *Pub. Astr. Soc. Pacific*, **86**, 616.
Bally, J., Langer, W., Stark, A.A., and Wilson, R.W. 1987, *Ap. J. (Letters)*, **312**, L45.
Barvainis R., Clemens, D.P., and Leach, R. 1988, *A.J.*, **95**, 510.
Bel, N. and Leroy, B. 1990, to appear in *Galactic and Extragalactic Magnetic Fields*, eds. R. Beck, P.P. Kronberg, and R. Wielebinski, (Dordrecht: Kluwer).
Burdyuzha, V.V. and Varshalovich. D.A. 1972, *Astron. Zh.*, **49**, 727.
Chandrasekhar, S. and Fermi, E. 1953, *Ap. J.*, **118**, 113.
Crutcher, R.M. 1979, *Ap. J.*, **234**, 881.
Crutcher, R.M. 1988, in *Molecular Clouds in the Milky Way and External Galaxies*, ed. Dickman, R.H., Snell, R., and Young, J., p. 105.
Deguchi, S. and Watson, W.D. 1984, *Ap. J.*, **285**, 126.
Deguchi, S. and Watson, W.D. 1990, *Ap. J.*, **354**, 649.
Draine, B.T. and Katz, N. 1986, *Ap. J.*, **310**, 392.
Elitzur, M., Hollenbach, D.J., and McKee, C. 1989, *Ap. .J.*, **346**, 983 (EHM).
Erickson, N.R., Goldsmith, P.J., Snell, R.L., Berson, R.L., Hugukenin, G.R., Ulich, B.L., and Lada, C. 1982, *Ap. J..*, **261**, L103.
Fiebig, D. and Güsten, R. 1989, *Astron. and Astrophys.*, **214**, 333.
Genzel, R., Reid, M.J., Moran, J.M., and Downes, D. 1981, *Ap. J.*, **244**, 884.
Goldreich, P., Keeley, D.A., Kwan, J.Y. 1973, *Ap. J.*, **179**, 111.
Gonatas, D.P., Hildebrand, R.H., Platt, S.R., Wu, X.D., Davidson, J.A., Novak, G., Aitken, D.K., and Smith, C. 1990, *Ap. J.*, submitted.
Goodman, A.A. 1989, Ph. D. Thesis, Harvard University.
Goodman, A.A., Crutcher, R.M., Heiles, C., Myers, P.C., and Troland, T.H. 1989, *Ap. J.*, **338**, L61.
Gredel, R., Lepp, S., Dalgarno, A., and Herbst, E. 1989, *Ap. J.*, **347**, 289.
Güsten, R. and Fiebig, D. 1990, to appear in *Galactic and Extragalactic Magnetic Fields*, eds. R. Beck, P.P. Kronberg, and R. Wielebinski, (Dordrecht: Kluwer).
Heiles, C. 1988, in *Galactic and Extragalactic Radio Astronomy*, eds. G.L. Verschuur and K.I. Kellerman, (New York: Springer-Verlag), p. 171.
Heiles, C. 1990, to appear in *Galactic and Extragalactic Magnetic Fields*, eds. R. Beck, P.P. Kronberg, and R. Wielebinski, (Dordrecht: Kluwer).
Heiles, C. 1988, *Ap. J.*, **324**, 321.
Heiles, C., Goodman, A.A., McKee, C.F., and Zweibel, E.G. 1990, in *Protostars and Planets III*, in press.
Heiles, C. and Stevens, M. 1986, *Ap. J.*, **301**, 331.

Heiles, C. and Troland, T.H. 1982, *Ap. J.*, **260**, L23.
Herbst, E. and Klemperer, W.B. 1973, *Ap. J.*, **185**, 505.
Hildebrand, R.H. 1988, *Q. Jl. R. Astr. Soc.*, **29**, 327.
Johnston, K.J., Migenes, V., and Norris, R.P. 1989, *Ap. J.*, **341**, 847 (JMN).
Knowles, S.H. and Batchelor, R.A. 1978, *Mon. Not. Royal Astr. Soc.*, **184**, 107.
Kylafis, N.D. 1983a, *Ap. J.*, **267**, 137.
Kylafis, N.D. 1983b, *Ap. J.*, **275**, 135.
Kylafis, N.D. and Shapiro, P.R. 1983, *Ap. J.*, **272**, L35.
Larson, R.B. 1981, *M.N.R.A.S.*, **194**, 809.
Lepp, S., Dalgarno, A., and Sternberg, A. 1987, *Ap. J.*, **321**, 383.
Leung, C.M., Herbst, E., and Huebner, W.F. 1984, *Ap. J. Suppl.*, **56**, 231.
Lis, D.C., Goldsmith, P.F., Dickman, R.L., Predmore, C.P., Omont, A., and Cernicharo, J. 1988, *Ap. J.*, **328**, 304.
McCutcheon, W.H., Vrba, F.J., Dickman, R.L., and Clemens, D.P. 1986, *Ap. J.*, **309**, 619.
McKee, C.F., Zweibel, E.G., Heiles, C., and Goodman, A.A. 1990, in *Protostars and Planets III*, in press.
Mitchell, G.F. and Watt, G.D. 1985, *Astron. Ap.*, **151**, 121.
Myers, P.C. and Goodman, A.A. 1990, in preparation (MG90).
Myers, P.C., Ho, P.T.P., Schneps, M.H., Chin, B., Pankonin, V., and Winnberg, A. 1978, *Ap. J.*, **220**, 864.
Nedoluha, G.E. and Watson, W.D. 1990, *Ap. J.*, **354**, 660.
Norris, R.P. 1984, *Mon. Not. Royal Astr. Soc.*, **207**, 127.
Novak, G., Gonatas, D.P., Hildebrand, R.H., Platt, S.R., and Dragovan, M. 1989, *Ap. J.*, **345**, 802.
Novak, G., Predmore, C.R., and Goldsmith, P.F. 1990, *Ap. J.*, **355**, 166.
Plambeck, R.L., Wright, M.C.H., Welch, W.J., Bieging, J.H., Baud, B., Ho, P.T.P., and Vogel, S.N. 1982, *Ap. J.*, **259**, 617.
Reid, M.J. and Moran, J.M. 1981, *Ann. Rev. Astron. Ap.*, **19**, 231.
Reid, M.J. and Silverstein, E.M. 1990, *Ap. J.*, submitted.
Solomon, P.M., Rivolo, A.D., Barrett, J., and Yahil, A. 1987, *Ap. J.*, **319**, 730.
Tielens, A.G.G.M. and Hollenbach, D., 1985, *Ap. J.*, **291**, 722.
Tomisaka, K., Ikeuchi, S., and Nakamura, E. 1988, *Ap. J.*, **335**, 239.
Troland, T.H. 1990. To appear in *Galactic and Extragalactic Magnetic Fields*, eds. R. Beck, P.P. Kronberg, and R. Wielebinski, (Dordrecht: Kluwer).
Troland, T.H., Crutcher, R.M., and Kazès 1986, *Ap. J.*, **304**, L57. Troland, T.H., Heiles, C., and Goss, W.M. 1989, *Ap. J.*, **337**, 342.
Turner, B.E. and Ziurys, L.M. 1988, in *Galactic and Extragalactic Radio Astronomy*, ed. G.L. Verschuur and K.I. Kellermann, 200.
van Dishoeck, E.F. and Black, J.H. 1986, *Ap. J. Suppl.*, **62**, 109.
Vogel, S.N., Wright, M.C.H., Plambeck, R.L., and Welch, W.J. 1984, *Ap. J.*, **283**, 655.
Wannier, P.G., Scoville, N.Z., and Barvainis, R. 1983, *Ap. J.*, **267**, 126.
Werner, M.W., Dinerstein, H.L., and Capps, R.W. 1983, *Ap. J.*, **265**, L13.
Wright, M.C.H., Plambeck, R.L. Vogel, S.N., Ho, P.T.P., and Welch, W.J. 1983, *Ap. J.*, **267**, L41.
Zweibel, E. 1990, *Ap. J.*, in press (20 Oct 1990).